coatings

MDPI

Article

Study on Deuterium Permeation Behavior of Palladium Films Prepared by Magnetron Sputtering Method

Zhihao Hong [1], Long Wang [1,*], Yongjin Feng [1,2], Baoping Gong [1], Jijun Yang [3] and Xiaoyu Wang [1,*]

[1] Southwestern Institute of Physics, Chengdu 610225, China; hongzhihao@swip.ac.cn (Z.H.); fengyj@swip.ac.cn (Y.F.); gongbp@swip.ac.cn (B.G.)
[2] Nuclear Power Institute of China, Chengdu 610041, China
[3] Key Laboratory of Radiation Physics and Technology of Ministry of Education, Institute of Nuclear Science and Technology, Sichuan University, Chengdu 610064, China; jjyang@scu.edu.cn
* Correspondence: wanglong@swip.ac.cn (L.W.); wangxy@swip.ac.cn (X.W.)

Abstract: Pre-depositing a Pd film is crucial for accurately acquiring the hydrogen permeability of metal materials, as it permits the production of ultra-pure hydrogen. However, the microstructure of Pd film and its effect on the hydrogen isotope permeation behavior of substrate materials have been neglected. In this study, Pd films were deposited on China Low-activation Ferritic (CLF−1) steel by magnetron sputtering. The effect of sputtering pressure on the microstructure and deuterium permeation behavior of Pd films at temperatures of 550−650 °C is presented. SEM results demonstrated that the films had a columnar crystal structure with a thickness of 0.6 ± 0.2 μm. The gas-driven permeation results revealed that the deuterium ion current intensity of the coated CLF−1 sample was at least three times lower than that of uncoated CLF−1 steel, which was influenced by the combined effect of oxygen and surface cracks. Oxygen could not be excluded from the films at a sputtering pressure of 10^{-3} Pa order of magnitude. It was also found that the films cracked during deuterium permeation experiments, which affected the deuterium permeation behavior. Films with large surface coverage and small grain sizes exhibited better cracking resistance. Our study provides promising insights into the hydrogen permeability of Pd films.

Keywords: Pd films; hydrogen gas–driven permeation; oxidation; grain size; cracking

Citation: Hong, Z.; Wang, L.; Feng, Y.; Gong, B.; Yang, J.; Wang, X. Study on Deuterium Permeation Behavior of Palladium Films Prepared by Magnetron Sputtering Method. *Coatings* **2022**, *12*, 978. https://doi.org/10.3390/coatings12070978

Academic Editor: Torsten Brezesinski

Received: 11 June 2022
Accepted: 6 July 2022
Published: 10 July 2022

1. Introduction

Tritium is an important fuel in thermonuclear D−T fusion reactors. It tends to permeate through structural materials into the environment and causes a critical issue in the tritium breeder blanket for realizing tritium self-sufficiency [1,2]. Tritium permeability is one of the most important parameters [3–7] of structural materials, such as reduced activation ferrite/martensitic (RAFM) steels, vanadium alloy, oxide dispersion strengthened (ODS) steel, etc. Generally, the surface of structural materials can be oxidized by surface chemical reactions at high temperatures during hydrogen isotope permeation tests [8,9]. The surface can become rough, and the surface oxides of structural materials can further hinder the absorption of molecular hydrogen (deuterium/tritium) [10,11], which affects the permeability testing results of gas-driven permeation experiments.

In order to acquire valid hydrogen isotope permeation data of metals, pre-deposited Pd films are adopted to avoid substrate oxidation during high-temperature permeation testing, according to reports. It was determined that a substrate with a 2.5 μm Pd coating can protect the freshly cleaned surface from being oxidized, and the permeability increased and the activation energy has been decreased compared to the oxidized surface [12]. Sun [13] found that the oxidization effect can be eliminated, and the hydrogen permeation process could be controlled by lattice diffusion for substrates being electroplated with Pd. Similar results were also presented by Huang, who showed that the surface of the steel without pre-deposited Pd films was oxidized, and the permeability was reduced by one order

of magnitude compared to that of Pd-coated steel [14]. However, few studies have paid attention to the quality of pre-deposited Pd film and its effect on the hydrogen isotope permeation behavior of the substrate materials. This is because many factors, such as the formation of PdO during the deposition of Pd films due to "target poison" by magnetron sputtering technology, unavoidable surface contaminations and cracks formed during thermal cycling application, and phase transition, intermetallic diffusion, defects, etc., can cause Pd films to have different hydrogen permeabilities.

In this work, we prepared Pd films by the magnetron sputtering method under different sputtering pressures and analyzed their effects on the microstructure and hydrogen isotope permeation behavior. The hydrogen isotope permeability was tested by a gas-driven permeation method. The structure and element changes in the Pd films were analyzed before and after deuterium permeation tests. Microstructural changes and their effects on the deuterium permeability of the films are presented.

2. Experimental Procedures

2.1. Sample Preparation

Reduced activation ferritic/martensitic (RAFM) steel was used as a substrate. The sample size of CLF−1 steel [15] was 12 mm in diameter with a thickness of 0.5 mm. The details of the substrate pre-treatment procedure are described in Ref. [16]. Before depositing, both sides of the substrate were first polished to a mirror finish, then cleaned in acetone and ethanol in an ultrasonic bath for 10 min and dried. The Pd coatings were deposited on one side (named upstream) of the mirror-polished CLF−1 substrate by physical vapor deposition (PVD) in a vacuum. Before depositing, the base vacuum in the chamber was 3×10^{-3} Pa. The deposition Ar pressure was set to four different values: 0.4 Pa, 0.6 Pa, 0.8 Pa and 1.0 Pa, respectively. The palladium target (99.95% purity) was pre-deposited for 600 s without opening the baffler of the target. For characterizing the thickness of Pd films, a monocrystalline silicon wafer was also used as a substrate. The films were fabricated at room temperature. The deposition current was 55 mA, and the deposition time was 900 s.

2.2. Deuterium Permeation Experiment and Methods

The deuterium permeation behavior of the samples was studied by using a gas-driven permeation apparatus. The detailed procedure of the permeation test is described in Ref. [17]. The deuterium pressure ranged from 30 kPa to 70 kPa in the upstream chamber. The deuterium permeation temperature ranged from 550 °C to 650 °C. The steady-state deuterium permeation flux can be calculated by Formula (1) [18]:

$$J = \frac{P \cdot p^n}{d} \quad (1)$$

where J is the deuterium permeation flux ($Pa \cdot m^3/s$). d is the film thickness (m). P is the permeability of deuterium through the material ($mol/(m \cdot s \cdot Pa^n)$). p is the driving pressure (Pa), and n is the pressure exponent. n is a constant for deuterium in a certain material, which is defined as 0.5 for a diffusion-limited process and 1 for a recombination reaction–limited process.

2.3. Characterization

The morphology of the films was characterized by a field-emission scanning electron microscope (FESEM, FEI Inspect F50, Hillsboro, OR, USA). The chemical composition was identified by using energy-dispersive X-ray spectroscopy (EDS, EDAX OCTANE SUPER, Pleasanton, CA, USA). The phase structure of the Pd films was analyzed by X-ray diffraction (XRD, Empyrean, PANalytical, Zaragoza, Spain) with an incidence angle of 1°.

3. Results and Discussion

3.1. Characterization of Pre-Deposited Pd Films

Figure 1 shows the cross-sectional SEM images of films deposited at different sputtering pressures. Nanoscale layers were formed on the substrate, indicating that films had been formed. They were dense, and no obvious cracks were formed along the crystal growth direction, which was perpendicular to the substrate surface. This suggests good adhesion between the film and the substrate. All films had a columnar structure, which is similar to previously reported work [19]. This proves that the growth modes of the grain were not affected by changing the sputtering vacuum in this study. The thicknesses of the films were measured to be about 0.6 ± 0.2 μm. As the sputtering vacuum increased, the thickness of the film increased slightly because of the increasing number of Ar^+. The deposition rates were 0.48 nm/s, 0.81 nm/s, 0.73 nm/s and 0.95 nm/s at sputtering pressures of 0.4 Pa, 0.6 Pa, 0.8 Pa and 1.0 Pa, respectively. As the growth rate of the film varies, the surface densification degree and grain size can differ [20], which can further influence the hydrogen permeability of the films.

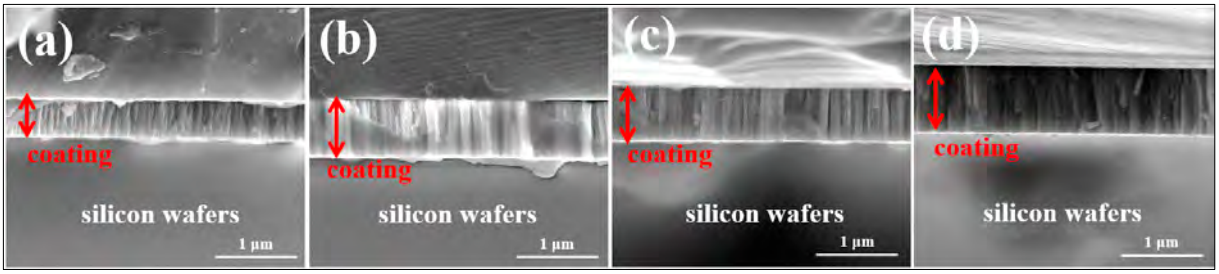

Figure 1. Cross-sectional images of films prepared at different sputtering pressures: (**a**) 0.4 Pa, (**b**) 0.6 Pa, (**c**) 0.8 Pa and (**d**) 1.0 Pa.

Figure 2 shows the surface morphologies and elemental composition of films deposited at different sputtering pressures. As Figure 2 depicts, all EDS spectrums presented the characteristic peak of Pd, revealing that all films were composed of Pd. This demonstrates that Pd atoms were successfully deposited on the substrate, corresponding to the cross-sectional SEM images shown in Figure 1. From the comparison, we found that the films had different surface morphologies. For the film prepared at a sputtering pressure of 0.4 Pa, the surface was dense, and no cracks could be found. Conversely, micro-cracks were formed on the surface of the films prepared at sputtering pressures of 0.6 Pa, 0.8 Pa and 1.0 Pa. Cracking can be an issue and cannot be neglected in high-temperature deuterium permeation tests (e.g., surface cracks may provide fast diffusion paths for deuterium permeation). Films with different surface densification degrees could have different hydrogen isotope permeabilities. Furthermore, the grain size distribution of the films was calculated using Image J software from the SEM images, as shown in Figure 3. The average grain sizes of the films prepared at sputtering pressures of 0.4 Pa, 0.6 Pa, 0.8 Pa and 1.0 Pa were 40.3 nm, 60.4 nm, 47.3 nm and 53.0 nm, respectively. The films deposited at sputtering pressures of 0.4 Pa and 0.8 Pa had smaller grain sizes, which could be a reason for the changes in deuterium permeation behavior.

However, the oxygen content in the film cannot be neglected. The elemental content of the films was analyzed by EDS, which revealed that the film was composed of O and Pd. The data are listed in Table 1. The reason for the existence of oxygen could be the presence of a small amount of residual oxygen during sputtering, as the base vacuum was in the order of magnitude of 10^{-3} Pa. A similar residual gas sputtering reaction pattern was also observed by Zhu et al. [21]. The phase structure of the films was further characterized by XRD. Figure 4 shows the XRD patterns of films prepared at different sputtering pressures. The solid vertical lines denoting diffraction peaks at 40.1° and 82.1° were indexed to (111) and (311) planes of the standard Pd phase with a cubic structure (reference PDF No. 46−1043 in the ICDD database). According to the analysis, all films had

a characteristic peak of Pd at 40.1°. For the films prepared at sputtering pressures of 0.4 Pa and 0.6 Pa, a new diffraction peak that was indexed to PdO (reference PDF No. 43−1024 in the ICDD database) appeared. Combined with the EDS results, the films were determined to be composed of Pd and O. The diffraction peak of PdO was not observed for the films prepared at sputtering pressures of 0.8 Pa and 1.0 Pa.

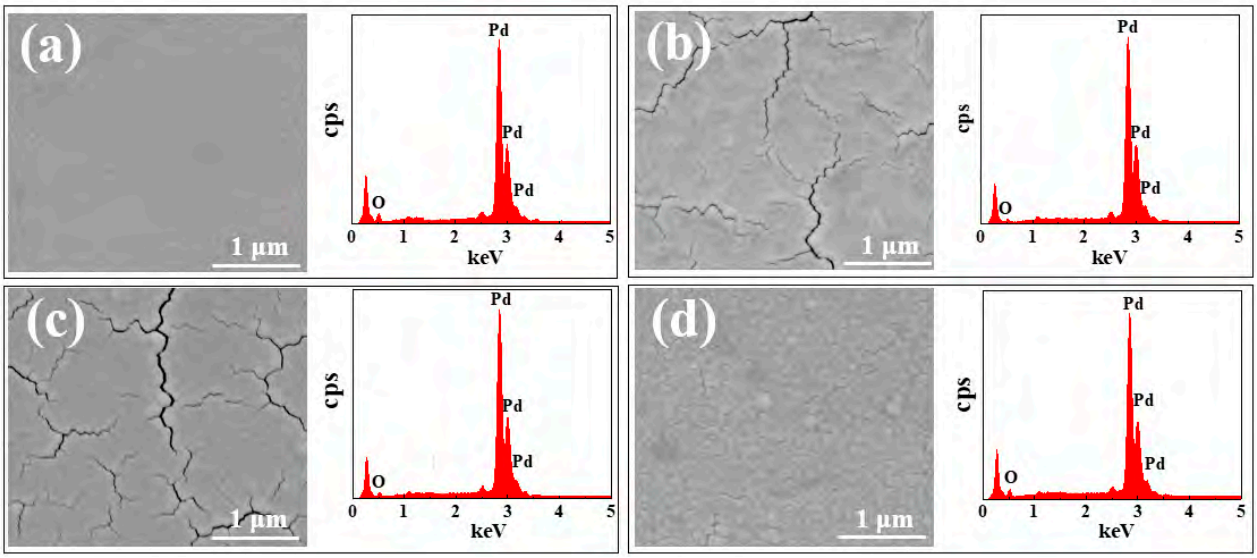

Figure 2. (**a**–**d**) Surface SEM and EDS images of films deposited at different sputtering pressures: (**a**) 0.4 Pa, (**b**) 0.6 Pa, (**c**) 0.8 Pa and (**d**) 1.0 Pa.

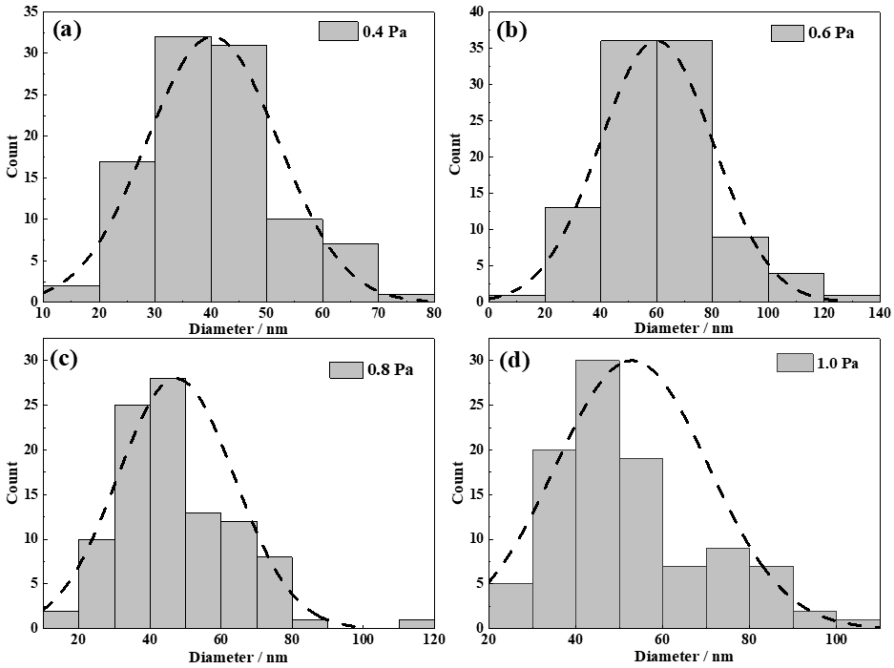

Figure 3. (**a**–**d**) Profile of grain size distribution of films prepared at different sputtering pressures: (**a**) 0.4 Pa, (**b**) 0.6 Pa, (**c**) 0.8 Pa and (**d**) 1.0 Pa.

Table 1. Surface chemical composition for samples before the tests: the values are in atomic percent (at. %).

Samples	Element Contents	
	Pd	O
0.4 Pa	59.39	40.61
0.6 Pa	79.59	20.41
0.8 Pa	72.62	27.38
1.0 Pa	61.69	38.31

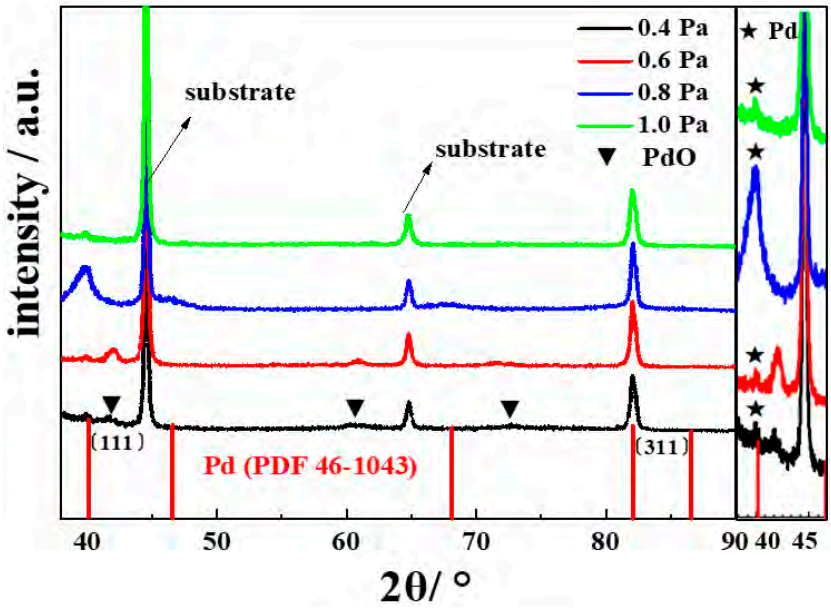

Figure 4. XRD patterns of films deposited at different sputtering pressures.

3.2. Deuterium Permeation Results

Figure 5 shows the deuterium ion current–time curves of the films at different temperatures and driving pressures. The deuterium ion current intensity increased with the increase in deuterium pressure, ranging from 30 kPa to 70 kPa. The curves rise gradually and reach a plateau. As the test temperature increased, the intensity of the steady permeation ion current increased. Compared with uncoated CLF–1 steel, the deuterium ion current intensity of the coated CLF−1 sample was at least three times lower. This could be the reason that the formation of PdO, which serves as a permeation barrier, trapped deuterium atoms and inhibited their permeation rate [22,23]. For films prepared at sputtering pressures of 0.6 Pa and 1.0 Pa, the deuterium ion current–time curves are similar at temperatures of 550 °C and 600 °C, but the film prepared at a sputtering pressure of 1.0 Pa had a higher deuterium ion current intensity at a temperature of 650 °C. This changing deuterium flux indicates the internal microstructural changes in the samples during the permeation test. For the film prepared at a sputtering pressure of 0.8 Pa, the deuterium ion current intensity was the lowest at temperatures ranging from 550 °C to 650 °C.

The pressure exponents of the coatings calculated by Equation (1) are shown in Figure 6. The results show that the pressure exponents (n) for all films were in the range of 0.67–0.94 at temperatures of 550−650 °C. It is assumed that the existence of O in the films could reduce the adsorption/dissociation kinetics of diatomic hydrogen [24]. Moreover, the Pd− and O− bonds can prevent the permeation of deuterium [24].

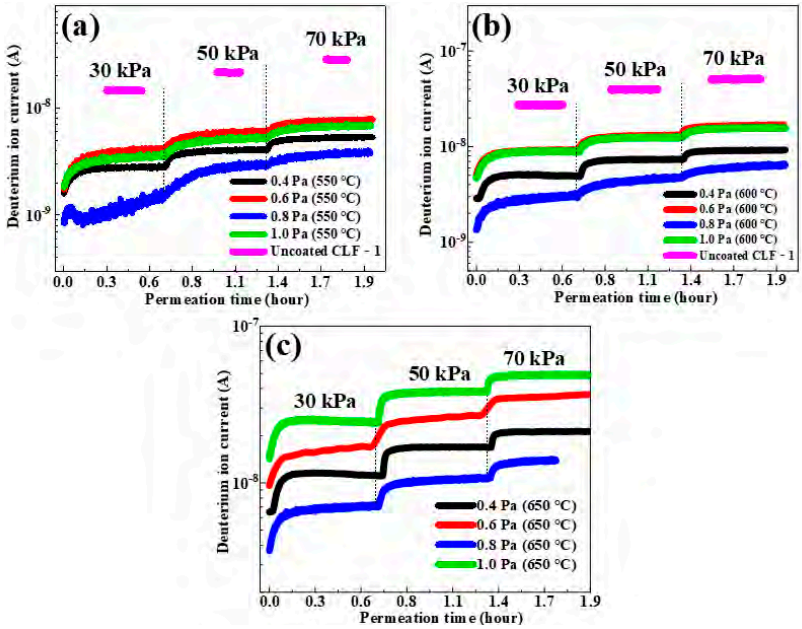

Figure 5. Deuterium ion current–time curves of Pd films at different temperatures and driving pressures: (**a**) 550 °C, 30–70 kPa; (**b**) 600 °C, 30–70 kPa; (**c**) 650 °C, 30–70 kPa.

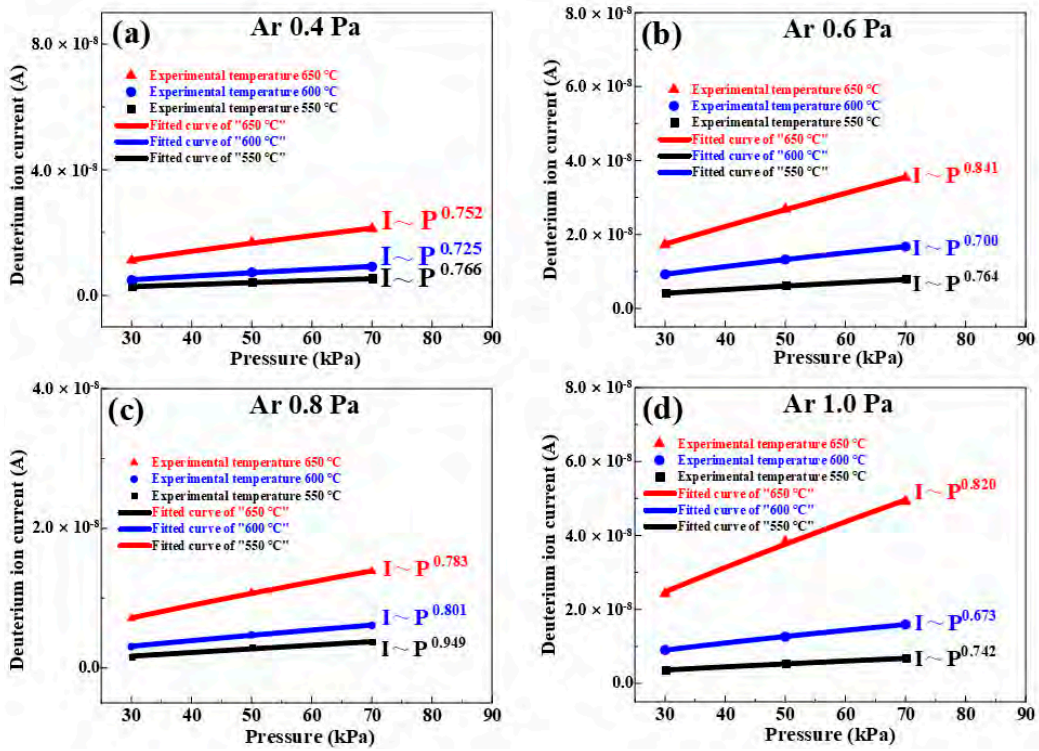

Figure 6. Driving pressure dependence of deuterium permeation ion current for Pd films: (**a**) 0.4 Pa, 550–650 °C; (**b**) 0.6 Pa, 550–650 °C; (**c**) 0.8 Pa, 550–650 °C; (**d**) 1.0 Pa, 550–650 °C.

3.3. Characterization after Deuterium Permeation

Figure 7 shows the surface SEM images of samples before and after deuterium permeation. The red region indicates the areas where the cracks are located. Surface coverages were calculated by Image J software. As Table 2 presents, the surface coverage of the films decreased from 99.98%, 97.19%, 93.12% and 99.12% to 97.61%, 85.72%, 91.22% and 86.01% for films deposited at pressures of 0.4 Pa, 0.6 Pa 0.8 Pa and 1.0 Pa, respectively. Films prepared at sputtering pressures of 0.6 Pa and 1.0 Pa had lower surface coverage. Combined

with the deuterium permeation data shown in Figure 5, it is reasonable to suppose that the higher deuterium permeation ion current intensity of the films prepared at sputtering pressures of 0.6 Pa and 1.0 Pa is caused by the increasing number of cracks because the cracks in these red regions will accelerate the deuterium permeation [25]. It was also found that the films with small grain sizes had better cracking resistance during deuterium permeation tests. In this case, deuterium atoms tended to be prevented from permeating through the films with small grain sizes. This is in agreement with the deuterium permeation results showing that the films prepared at sputtering pressures of 0.4 Pa and 0.8 Pa had a lower deuterium permeation ion current intensity.

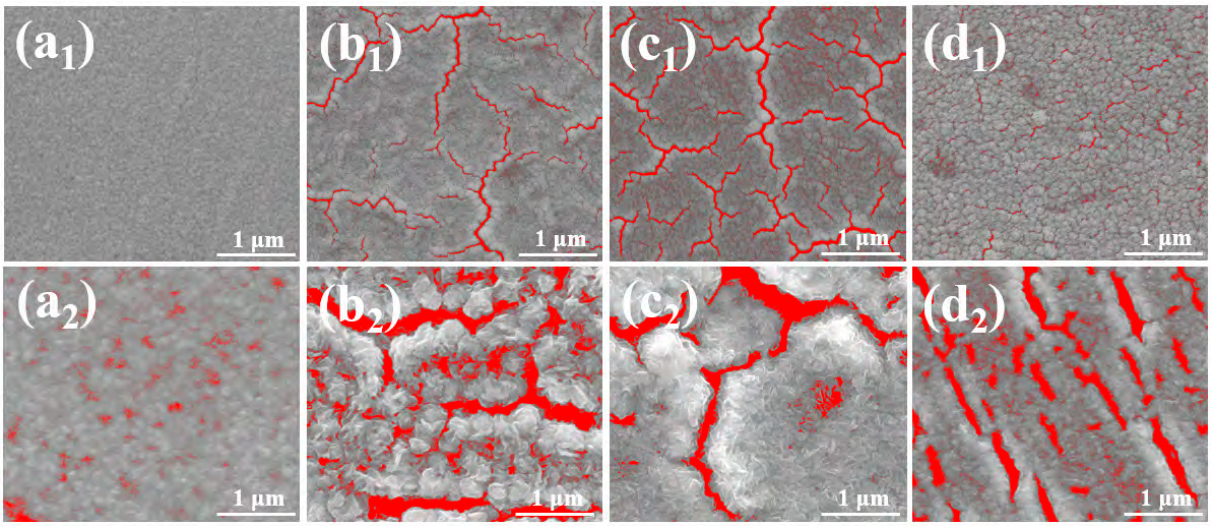

Figure 7. SEM images of films processed by Image J: (**a1**–**d1**) 0.4 Pa, 0.6 Pa, 0.8 Pa and 1.0 Pa before deuterium permeation; (**a2**–**d2**) 0.4 Pa, 0.6 Pa, 0.8 Pa and 1.0 Pa after deuterium permeation.

Table 2. Surface coverages of the films before and after deuterium permeation tests.

Samples	Surface Coverage %			
	0.4 Pa	**0.6 Pa**	**0.8 Pa**	**1.0 Pa**
Pre-deposited	99.98	97.19	93.12	99.12
After permeation tests	97.61	85.72	91.22	86.01

Figure 8 shows the EDS results of films after deuterium permeation tests. The O and Pd elements were homogeneously distributed and demonstrated that oxidation formed on the Pd films. Table 3 shows the surface chemical composition for all samples after the tests. As the table presents, increases in O were 20.39 at. %, 57.63 at. %, 44.92 at. % and 27.40 at. % for films prepared at sputtering pressures of 0.4 Pa, 0.6 Pa, 0.8 Pa and 1.0 Pa after deuterium permeation tests, respectively. Pre-deposited films with large surface coverage showed lower surface oxygen content during deuterium permeation tests. Moreover, the surfaces of Pd films with smaller grain sizes showed better oxidation resistance. This confirmed that oxygen could be introduced to the Pd films, which further reacts with the films during the permeation [26]. In conclusion, pre-deposited films with large surface coverage and small grain sizes had better cracking resistance.

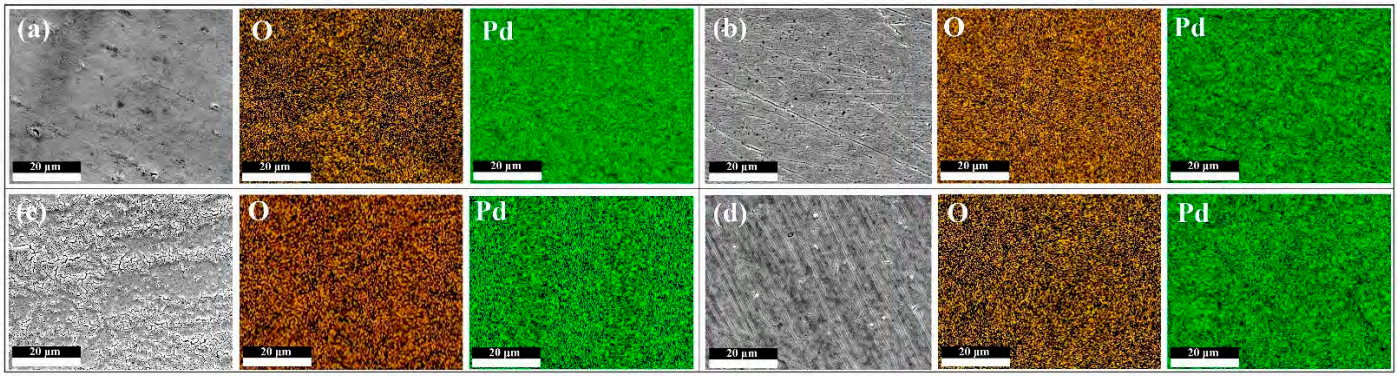

Figure 8. (**a**–**d**). EDS mapping of the pre-deposited Pd film deposited at different sputtering pressures after deuterium permeation: (**a**) 0.4 Pa, (**b**) 0.6 Pa, (**c**) 0.8 Pa and (**d**) 1.0 Pa.

Table 3. Surface chemical composition of samples after the tests: the values are in atomic percent (at. %).

Samples	Element Contents		
	Pd	O	O Content Changes Compared to the Deposited Ones
0.4 Pa	39.00	61.00	+20.39
0.6 Pa	21.96	78.04	+57.63
0.8 Pa	27.70	72.30	+44.92
1.0 Pa	34.29	65.71	+27.40

4. Conclusions

In this study, Pd films were deposited on CLF−1 steel by magnetron sputtering. The effects of the sputtering pressure on the microstructure and deuterium permeation behavior of films at 550−650 °C are presented. SEM results demonstrated that the films had a columnar crystal structure with a thickness of 0.6 ± 0.2 μm. The gas-driven permeation results revealed that the deuterium ion current intensity of coated CLF−1 samples was at least three times lower than that of uncoated CLF−1 steel, which was influenced by a combination of oxygen and surface cracks, according to the tests. Oxygen could not be excluded from the films at a sputtering pressure of 10^{-3} Pa order of magnitude. It was also found that the films underwent cracking during deuterium permeation, which affected the deuterium permeation behavior. Films with large surface coverage and small grain sizes exhibited better cracking resistance. However, the preparation parameters should be further optimized to acquire Pd films with good adhesion and high uniformity during hydrogen permeation tests at high temperatures. The effects of structural changes and oxygen concentration should also be studied thoroughly in the future. Our study provides promising insights into the hydrogen permeability of Pd ultrathin films.

Author Contributions: Conceptualization, L.W.; funding acquisition, L.W.; investigation, Z.H.; methodology, Z.H.; resources, X.W. and L.W.; supervision, L.W. and Y.F.; writing—original draft, Z.H.; writing—review and editing, L.W., Y.F., B.G. and J.Y. All authors have read and agreed to the published version of the manuscript.

Funding: This work was supported by the National Natural Science Foundation of China (Grant No.12005051).

Institutional Review Board Statement: Not applicable.

Informed Consent Statement: Not applicable.

Data Availability Statement: Data sharing is not applicable to this article.

Conflicts of Interest: The authors declare no conflict of interest.

References

1. Coenen, J.W.; Antusch, S.; Aumann, M.; Biel, W.; Du, j.; Engels, J.; Heuer, S.; Houben, A.; Hoeschen, T.; Jasper, B.; et al. Materials for DEMO and reactor applications–boundary conditions and new concepts. *Phys. Scr.* **2016**, *2016*, 014002. [CrossRef]
2. Chen, C.A.; Zhou, X.; Wang, Z.L.; Wang, B.; Liu, L.b.; Xiang, X.; Yong, Y.; Song, J.F. Assessment of Tritium Release Through Permeation and Natural Leakage in ITER CN HCCB TBS Under Normal Operations. *Fusion Sci. Technol.* **2018**, *73*, 34–42. [CrossRef]
3. Long Wang, L.; Yang, J.J.; Liang, C.H.; Feng, Y.J.; Jin, W.; Cao, J.L.; Wang, X.Y.; Feng, K.M.; Kleyn, A.W.; Liu, N. Preparation and properties of improved Al_2O_3 based MOD coatings as tritium permeation barrier. *Fusion Eng. Des.* **2019**, *143*, 233–239. [CrossRef]
4. Zhou, H.S.; Hirooka, Y.; Ashikawa, B.; Muroga, T.; Sagara, A. Gas- and plasma-driven hydrogen permeation through a reduced activation ferritic steel alloy F82H. *J. Nucl. Mater.* **2014**, *455*, 470–474. [CrossRef]
5. Wang, B.; Liu, L.B.; Xiang, X.; Rao, Y.C.; Ye, X.Q.; Chen, C.A. Diffusive transport parameters of deuterium through China reduced activation ferritic-martensitic steels. *J. Nucl. Mater. Asp. Fission Fusion* **2016**, *47*, 30–33. [CrossRef]
6. Alimov, V.K.; Hatano, Y.J.; Sugiyama, K.; Kondo, S.; Hinoki, T.; Tokitani, M. Influence of displacement damages on deuterium retention in reduced activation ferritic/martensitic steels F82H and Eurofer97-ScienceDirect. *Fusion Eng. Des.* **2016**, *113*, 336–339. [CrossRef]
7. Oyaidzu, M.; Isobe, K.; Nakamura, H.; Hayashi, T.; Yamanishi, T. Permeation behavior of tritium through F82H steel. *J. Nucl. Mater.* **2011**, *417*, 1143–1146. [CrossRef]
8. Rouillard, F.; Cabet, C.; Wolski, K.; Pijolat, M. Oxidation of a chromia-forming nickel base alloy at high temperature in mixed diluted CO/H_2O atmospheres. *Corros. Sci.* **2009**, *51*, 752–760. [CrossRef]
9. Tanaka, T.; Chikada, T.; Hishinuma, Y.; Takeo, M.; Akio, S. Formation of Cr_2O_3 layers on coolant duct materials for suppression of hydrogen permeation. *Fusion Eng. Des.* **2017**, *124*, 1046–1051. [CrossRef]
10. Dolinsky, Y.N.; Zouev, Y.N.; Lyasota, I.A.; Saprykina, I.V.; Sagaradz, V.V. Permeation of deuterium and tritium through the martensitic steel F82H. *J. Nucl. Mater.* **2002**, *307*, 1484–1487. [CrossRef]
11. Takumi, C.; Keisuke, K.; Jumpei, M.; Seira, H.; Moeki, M.; Hikari, F.; Kouhei, O.; Teruya, T.; Yoshimitsu, H.; Yoshiteru, S. Surface oxidation effect on deuterium permeation in reduced activation ferritic/martensitic steel F82H for DEMO application-ScienceDirect. *Fusion Eng. Des.* **2019**, *146*, 450–454.
12. Swansiger, W.A.; Mills, B.E.; Nagelberg, A.S. Deuterium permeation through oxidized fecralloy. *J. Nucl. Mater.* **1984**, *123*, 1292–1297. [CrossRef]
13. Sun, X.K.; XU, J.; LI, Y.Y. Hydrogen permeation behaviour in austenitic stainless steels. *Mater. Sci. Eng.* **1989**, *114*, 179–187.
14. Huang, H.T.; Zheng, J.P.; Ding, S.; Wang, W.J.; Zhang, H.F. Effect of natural oxide film on the deuterium permeation behavior of 430 stainless steel. *Fusion Eng. Des.* **2020**, *152*, 111469. [CrossRef]
15. Liao, H.B.; Wang, X.Y.; Yang, G.P.; Feng, Y.J.; Wang, P.H.; Feng, K.M. Recent progress of R&D activities on reduced activation ferritic/martensitic steel (CLF–1). *Fusion Eng. Des.* **2019**, *147*, 111235.
16. Hong, Z.H.; Wang, L.; Zhang, W.; Yang, J.; Feng, Y.J.; Yang, J.J.; Li, H.X.; Yin, H.Q.; Zhang, L.; Wang, X.Y. Hydrogen Isotope Permeation Behavior of AlCrFeTiNb, AlCrMoNbZr and AlCrFeMoTi High-Entropy Alloys Coatings. *Coatings* **2022**, *12*, 171. [CrossRef]
17. Wang, L.; Zhang, W.; Chen, X.D.; Luo, X.F.; Feng, Y.J.; Gong, B.P.; Wang, X.Y.; Yang, J.J. Corrosion of reduced activation ferritic-martensitic steel CLF-1 by Li_2TiO_3 in ambient air-ScienceDirect. *Fusion Eng. Des.* **2021**, *173*, 112856. [CrossRef]
18. Johnson, H.H. Hydrogen in iron. *Metall. Trans. B* **1988**, *19*, 2371–2387. [CrossRef]
19. Tucho, W.M.; Venvik, H.J.; Walmsley, J.C.; Stange, M.; Ramachandran, A.; Mathiesen, R.H.; Borg, A.; Bredesen, R.; Holmestad, R. Microstructural studies of self-supported (1.5–10 μm) Pd/23 wt% Ag hydrogen separation membranes subjected to different heat treatments. *J. Mater. Sci. Lett.* **2009**, *44*, 4429–4442. [CrossRef]
20. Yan, H.; Dittmeyer, R. Preparation of thin palladium membranes on a porous support with rough surface. *J. Membrane Sci.* **2007**, *302*, 160–170.
21. Zhu, S.F.; Wu, Y.P.; Liu, T.W.; Wang, X.; Yan, J.W.; Yin, A.Y. Interface structure and deuterium permeation properties of Er_2O_3/SiC multilayer film prepared by RF magnetron sputtering. *Int. J. Hydrogen Energy* **2015**, *40*, 5701–5706. [CrossRef]
22. Titkov, A.I.; Salanov, A.N.; Koscheev, S.V.; Boronin, A.I. Mechanisms of Pd (1 1 0) surface reconstruction and oxidation: XPS, LEED and TDS study. *Surf. Sci.* **2006**, *600*, 4119–4125. [CrossRef]
23. Engels, J.; Houben, A.; Linsmeier, C. Hydrogen isotope permeation through yttria coatings on Eurofer in the diffusion limited regime-ScienceDirect. *Int. J. Hydrogen Energ.* **2021**, *46*, 13142–13149. [CrossRef]
24. Fuerst, T.F.; Humrickhouse, P.W.; Taylor, C.N.; Shimada, M. Surface effects on deuterium permeation through vanadium membranes. *J. Membr. Sci.* **2021**, *620*, 118949. [CrossRef]
25. Pisarev, A.; Tsvetkov, I.; Yarko, S. Hydrogen permeation through membranes with cracks in protection layer. *Fusion Eng. Des.* **2007**, *82*, 2120–2125. [CrossRef]
26. Keurentjes, J.; Gielens, F.C.; Tong, H.D. High-Flux Palladium Membranes Based on Microsystem Technology. *Ind. Eng. Chem. Res.* **2004**, *43*, 4768–4772. [CrossRef]